объединенный
институт
ядерных
исследований
дубна

E1-93-133

NUCLEAR STRUCTURE FUNCTIONS IN CARBON NEAR $x = 1$

BCDMS Collaboration

Submitted to "Nuclear Physics A"

1993

1 Introduction

The structure functions of nucleons which describe the distribution of quarks inside nuclear matter have been measured, for both free and bound nucleons, in a variety of high precision experiments with electron, muon, and neutrino beams [1]–[9]. In these measurements, it has been observed that the structure function $F_2^A(x, Q^2)$ of a nucleus A, and consequently the quark distributions measured in complex nuclei, is different from the structure function of a free nucleon [6, 11].

Most of the experimental data on structure functions of nuclear targets have been measured below $x = 0.8$, where x is the Bjorken scaling variable. However, many effects predicted by nuclear models such as the high momentum component of Fermi motion, few nucleon correlations, multiquark clusters etc., are expected to manifest themselves mostly in the region close to $x = 1.0$, which is the kinematic limit for a lepton scattered from a free nucleon. Due to substantial experimental difficulties, this kinematic region has remained almost unexplored so far. Upper limits on F_2^A from a measurement of deep inelastic neutrino scattering on iron have been given in ref. [10]. Measurements from electron scattering on nuclear targets at lower beam energies have recently been reported [12].

In this paper, we report on the first experimental measurement of the bound nucleon structure function $F_2^C(x, Q^2)$ at large squared four-momentum transfer Q^2, in the region $x > 0.8$. The data were obtained in deep inelastic scattering of a beam of 200 GeV muons on a carbon target. The analysis of data in the range $0.25 < x < 0.8$ from the same experiment has been reported in [1].

2 Cross section and nucleon structure functions

In the experiment described here, the quark structure of a nucleus of mass A is probed in the inclusive deep inelastic scattering reaction

$$\mu + A \rightarrow \mu' + X, \tag{1}$$

where μ' is the scattered muon and X is the hadronic final state. The dominant contribution to the cross section of reaction (1) comes from single photon

exchange. In this approximation, the double differential cross section can be written as

$$\frac{1}{A}\frac{d^2\sigma_0}{dQ^2dx} = \frac{4\pi\alpha^2}{Q^4x}\left[1-y-\frac{Q^2}{4E^2}+\frac{y^2E^2+Q^2}{2E^2[R^A(x,Q^2)+1]}\right]F_2^A(x,Q^2), \quad (2)$$

where α is the electromagnetic coupling constant, E is the energy of the incident muon, Q^2 is the squared four momentum transfer from the muon to the nucleus, x and y are the Bjorken scaling variables and $F_2^A(x,Q^2)$ and $R^A(x,Q^2)$ are the structure functions of the nucleus. We follow the convention that the structure functions are normalized to the number of nucleons in the nucleus.

In the laboratory frame, the Lorentz invariant variables Q^2, x and y are related to measurable quantities by the expressions:

$$Q^2 = 4EE'\sin^2(\theta/2), \quad (3)$$

$$\nu = E - E', \quad (4)$$

$$x = \frac{Q^2}{2M\nu}, \quad y = \frac{\nu}{E}, \quad (5)$$

where E' is the energy of scattered muon, θ is the scattering angle, and M is the mass of the target particle. When M is taken to be the nucleon mass, then $0 \leq x \leq A$ and F_2^A is defined in the same interval.

The structure function $R^A(x,Q^2) = \sigma_L^A/\sigma_T^A$ is the ratio of absorption cross sections for virtual photons of longitudinal and transverse polarization. We have shown in ref. [1] that in the region $Q^2 > 40\,\mathrm{GeV}^2$ and $0.25 < x < 0.8$ this structure function is compatible with zero, $R^C = 0.015 \pm 0.013\,(\mathrm{stat.}) \pm 0.026\,(\mathrm{syst.})$. This measurement is also compatible with perturbative Quantum Chromodynamics (QCD) calculations which predict R to decrease with x and Q^2 and to become small in the kinematic region of our measurement [13]. Furthermore, the contribution of R to the cross section (2) decreases with increasing x except for very large values of y which are excluded from the present analysis. We therefore conclude that R can be safely assumed to be zero in the analysis of $F_2^A(x,Q^2)$ in our kinematic range.

3 Apparatus and data taking

The data were collected with a high luminosity spectrometer in the CERN SPS muon beam. The experimental apparatus is shown in Fig. 1 and has

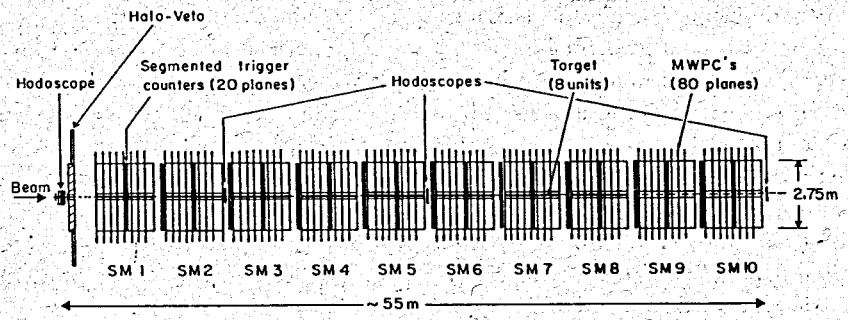

Fig. 1: Schematic view of the spectrometer.

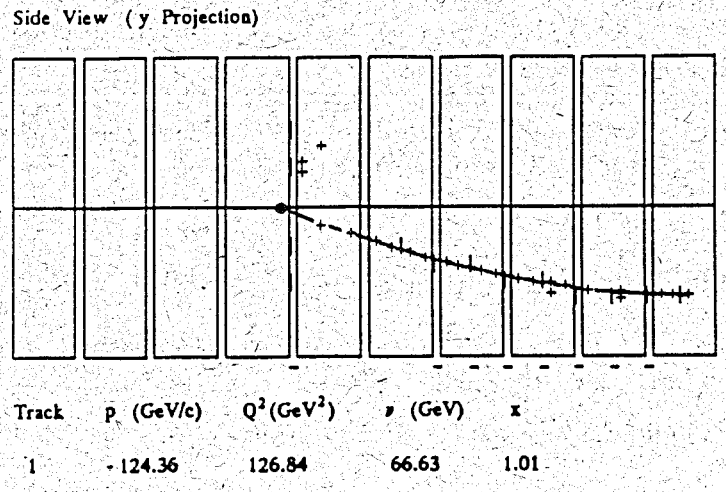

Fig. 2: Typical large x event.

been described in detail elsewhere [14]. It consisted of a 50 m long segmented toroidal iron magnet which was magnetized close to saturation and surrounded a 40 m long carbon target. The hadronic shower produced in the deep inelastic interaction was absorbed by the target and by the spectrometer iron within a few meters from the interaction point and the surviving scattered muon was focused towards the spectrometer axis. The toroids were equipped with twenty planes of trigger counters segmented into concentric rings around the beam axis to permit a Q^2 selective trigger, and with 80 planes of MWPC measuring the track in two orthogonal projections. Four hodoscopes along the spectrometer axis detected the incoming muons and measured their trajectories. A wall of scintillation counters in front of the spectrometer provided a veto against the beam halo.

The momenta of the incident muons were measured with a spectrometer consisting of an air-gap magnet and four scintillator hodoscopes in the beam line. The average energy of the incident beam was 200 GeV. Due to energy loss in the target, the average muon energy at the interaction point was 194 Gev. The beam intensity was typically $2 \cdot 10^7$ μ per 1.4 sec beam spill from the accelerator, and was counted with the beam hodoscopes using two different methods [14]. After corrections for deadtime, the results obtained by the two methods agreed to $\approx 1\%$. The total number of incident muons used for this measurement was $(4.23 \pm 0.13) \cdot 10^{11}$.

The trigger required signals from four consecutive trigger planes situated anywhere in the apparatus, corresponding to scattered muon tracks longer than 8 m, in coincidence with a beam signal and in anticoincidence with the halo signal.

4 Event reconstruction

The recorded events were processed using the program PATRAC [15] with the following steps:

- pattern recognition and event reconstruction;
- selection of events;
- computation of detector efficiencies;

- computation of the incident muon flux and corrections for dead time losses.

The kinematic reconstruction determined the scattered muon momentum and the scattering angle θ. In the event selection, each track was required to have at least 4 points measured in each projection and 10 points in total; the average number of points in each projection was 28. The vast majority of events has a simple topology of a single scattered muon track. A typical event is shown in Fig. 2.

The rejection of background from halo feed-through and accidental tracks was based on geometrical and timing cuts and the requirement that the tracks had to be geometrically consistent with the trigger pattern recorded by the scintillation counters. Only about 2% of the events could not be unambiguously identified as good or background and were scanned visually. About half of the scanned events were found to be good. The misidentification of background events as good events, and of good events as background, was found to be less than 0.1% by visual scanning of control samples of both categories.

Only data taking runs with a stable performance of the beam and of all detectors were retained for the final analysis. This requirement led to a rejection of about 10% of the raw data. The events selected for the calculation of structure functions had to fulfill the following criteria:

- the interaction vertex is contained in the fiducial volume of the target;
- the scattered muon track is contained in the fiducial volume of the spectrometer;
- the reconstructed events have $E' > 30\,\mathrm{GeV}$, $Q^2 > 52\,\mathrm{GeV}^2$, and $0.4 < x < 1.8$. In this region, the geometrical acceptance of the spectrometer is flat in x and Q^2 and is everywhere larger than 65%;
- the reconstructed events are observed in a region of good resolution in the scattering angle θ ($\theta > 0.045\,\mathrm{rad}$).

After these cuts we obtain $7.6 \cdot 10^4$ events for the analysis of structure functions. Of these, 1356 events are reconstructed in the range $x > 0.8$. We have retained the events with $0.4 < x < 0.8$ for comparison with the results reported in [1] which were obtained with a somewhat different method.

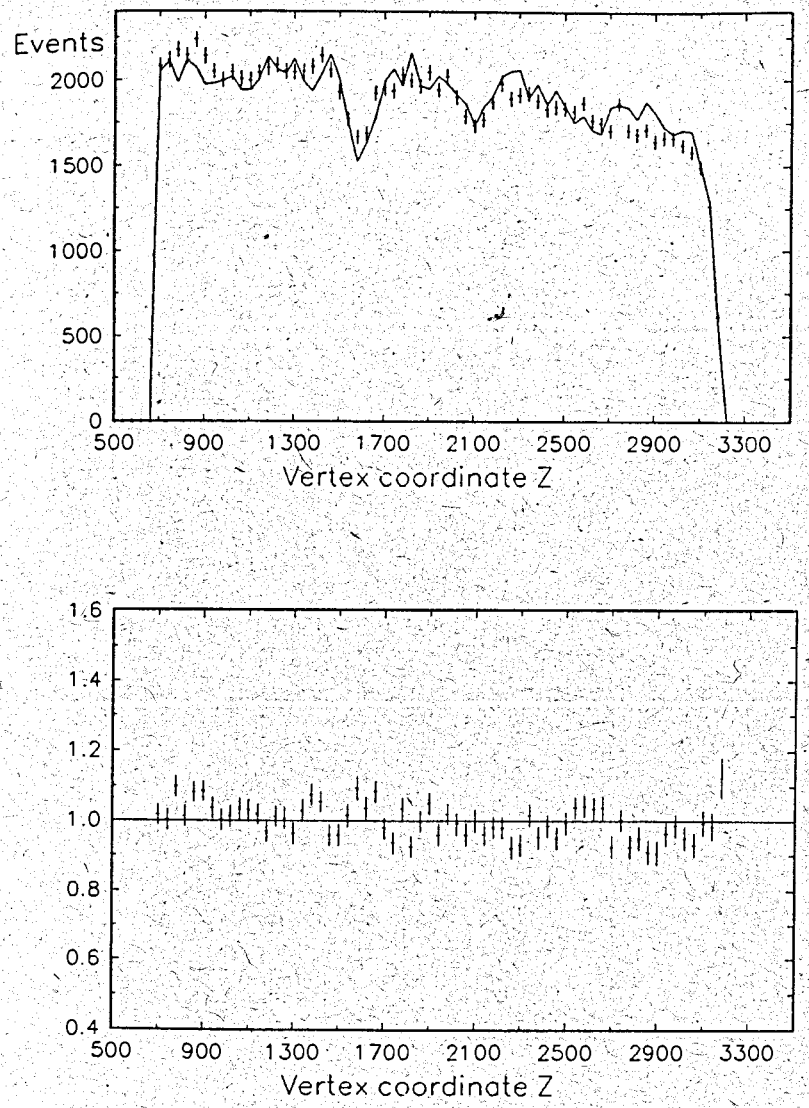

Fig. 3: Comparison of experimental (points) to Monte Carlo (solid line) event distributions: (a) distribution of the reconstructed interaction vertex along the beam direction; (b) azimuth angle ϕ of the scattered muon. These variables are independent of the kinematic variables.

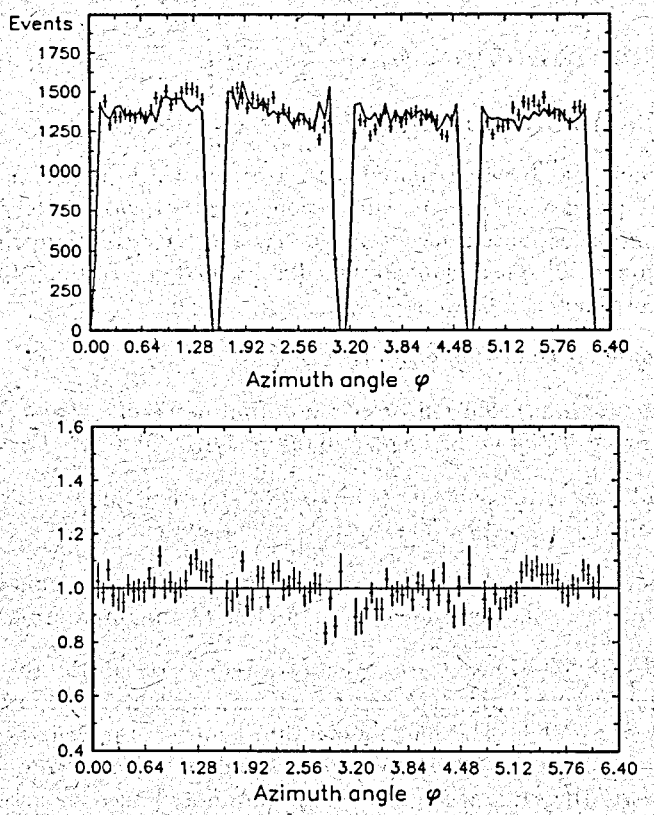

Fig. 3b

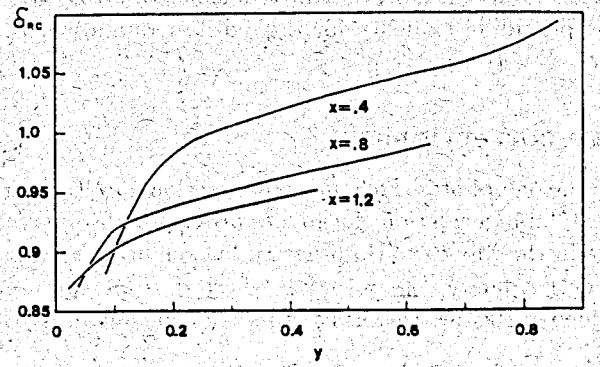

Fig. 4: The radiative correction factor δ_{RC} as a function of y, for different values of x.

5 Determination of $F_2^C(x, Q^2)$

Monte Carlo simulation of the experiment

The experiment has been simulated with a Monte Carlo program based on the GEANT package [16]. This simulation serves to correct the measured differential cross section for acceptance losses and for resolution smearing of the spectrometer. The program contained a detailed description of the beam and the spectrometer, including:

- the phase space of the incoming beam;
- efficiencies and resolution properties of all detectors. Typical efficiencies were $\approx 97\%$ for the trigger counters and $\approx 98\%$ for the MWPC's;
- multiple scattering and energy loss of both incident and scattered muons, including the statistical fluctuations of energy losses [17];
- additional detector hits from δ rays generated along the muon track and from hadronic shower punch-through close to the interaction vertex.

A sample of 110 000 Monte Carlo events was generated in the region $0.8 < x \leq 1.8$; the Monte Carlo data generated for the analysis reported in [1] were used for $x \leq 0.8$. The four-momentum transfer was generated in the interval $30\,\mathrm{GeV}^2 \leq Q^2 \leq 260\,\mathrm{GeV}^2$. The simulated events were processed through exactly the same reconstruction program and event selection as the experimental data.

The quality of the simulation procedure has been checked by comparing experimental and simulated event distributions. A good agreement is observed, thus providing evidence for a good understanding of the apparatus (Fig. 3).

Radiative corrections

To evaluate the one-photon exchange cross section and to determine F_2^C from the measured data, corrections for higher order processes have to be applied. This is done in the Monte Carlo program by weighting each generated event with a correction factor $\delta_{RC} = \sigma/\sigma_0$, where σ is an approximation to the measured deep inelastic scattering cross section and σ_0 is the one-photon exchange cross section of eq. (2). The same corrections as described in ref. [1] have been used for $x \leq 1$. For $x > 1.0$, only the lepton line corrections from refs. [18] have been applied, replacing the nucleon mass M by $2M$ in all kinematic relations to account for the fact that the scattering may partly occur on substructures larger than a nucleon. Corrections to the hadron line and from electroweak interference have been neglected since they depend on the quark dynamics which are poorly known in this kinematic region. They are estimated to be smaller than 2% of the cross section. The parametrisation of $F_2^C(x, Q^2)$ used for the calculation of δ_{RC} was the same as given in eqs. (7) and (8) below. For a few typical values of x and y, $\delta_{RC}(x, y)$ is shown in Fig. 4.

Evaluation of $F_2^C(x, Q^2)$

Due to the resolution of the spectrometer, an event with true variables (x, Q^2) is reconstructed with variables $(x', Q^{2'})$. The density of registered events $N_r(x', Q^{2'})$ is related to the differential cross section $d^2\sigma/dxdQ^2$ by

$$N_r(x', Q^{2'}) = \mathcal{L} \int_x \int_{Q^2} dx dQ^2 \frac{d^2\sigma}{dx dQ^2} \epsilon(x, Q^2) \rho(x, x', Q^2, Q^{2'}), \qquad (6)$$

where the luminosity $\mathcal{L}$ is the product of the muon flux and the number of nucleons in the target, $\epsilon(x, Q^2)$ is the geometric acceptance, and $\rho(x, x', Q^2, Q^{2'})$ is the resolution function of the apparatus, i.e. the probability density to observe an event with true variables $(x; Q^2)$ at $(x', Q^{2'})$.

The acceptance function $\epsilon(x, Q^2)$ and the resolution function $\rho(x,x',Q^2,Q^{2'})$ are determined from the Monte Carlo simulation. In the presence of significant resolution smearing, and with a finite number of Monte Carlo events, it is difficult to construct an explicit mathematical description of ρ. It is therefore customary to evaluate $d^2\sigma/dxdQ^2$, and thus $F_2(x, Q^2)$, from eq. (6) with an iterative method as described in [1].

For the present analysis, we have adopted a simplified procedure for the F_2 evaluation which is better adapted to the limited statistical accuracy of the data. It consists in a direct comparison of the experimental and Monte Carlo event distributions, using in the simulation – i.e. in the right hand side of eq. (6) – trial structure functions which differ from the previously

Table 1: *The structure function F_2^C per nucleon measured in this experiment, as a function of x and Q^2. The statistical error is given by ΔF_2. The f_i indicate the different systematic errors discussed in the text; they are given as multiplicative factors by which F_2^C has to be multiplied or divided. The upper limits for $x \geq 1.15$ are given for a confidence level of 90%. The absolute normalisation uncertainty of the data is smaller than 3%.*

x	Q^2 (GeV^2)	F_2 (10^{-6})	ΔF_2 (10^{-6})	f_r	f_b	f_s	f_d
0.85	61	1560	94	1.160	1.055	1.093	0.997
	85	1260	69	1.096	1.036	1.068	0.999
	150	1090	78	1.060	1.010	1.043	0.999
0.95	61	266	23	1.240	1.110	1.140	0.997
	85	258	19	1.163	1.075	1.102	0.999
	150	261	28	1.105	1.022	1.070	0.999
1.05	61	64.1	7.4	1.320	1.202	1.203	0.998
	85	47.8	5.2	1.238	1.137	1.149	0.999
	150	45.8	5.1	1.176	1.046	1.109	0.999
1.15	61	< 27.0					
	85	< 15.1					
	150	< 22.3					
1.30	61	< 6.9					
	85	< 5.4					
	150	< 3.8					

Table 2: *Results on the slope parameter s for $x > 0.8$. Δs indicates statistical and systematic errors combined in quadrature*

Q^2 (GeV^2)	s	Δs
$52 - 70$	16.8	$^{+1.7}_{-0.6}$
$70 - 100$	16.9	$^{+1.3}_{-0.6}$
$100 - 200$	16.3	$^{+0.8}_{-0.6}$
$52 - 200$	16.5	$^{+0.6}_{-0.6}$

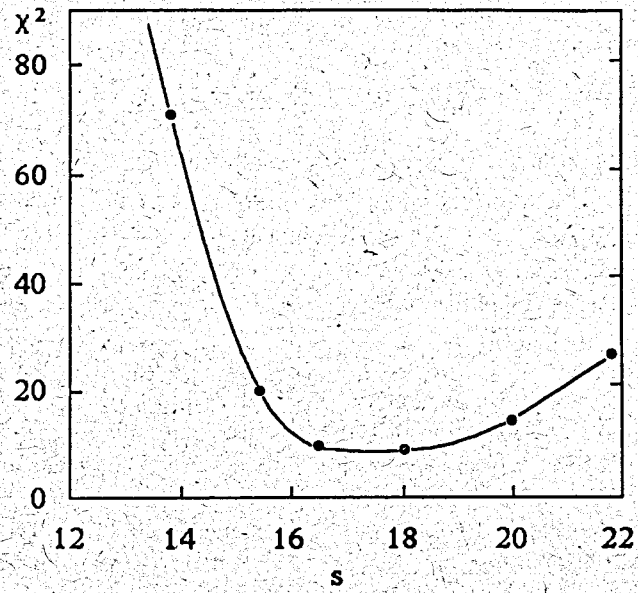

Fig. 5: The χ^2 of the comparison of the carbon data with the Monte Carlo events for $x > 0.7$ as a function of the parameter s discussed in the text.

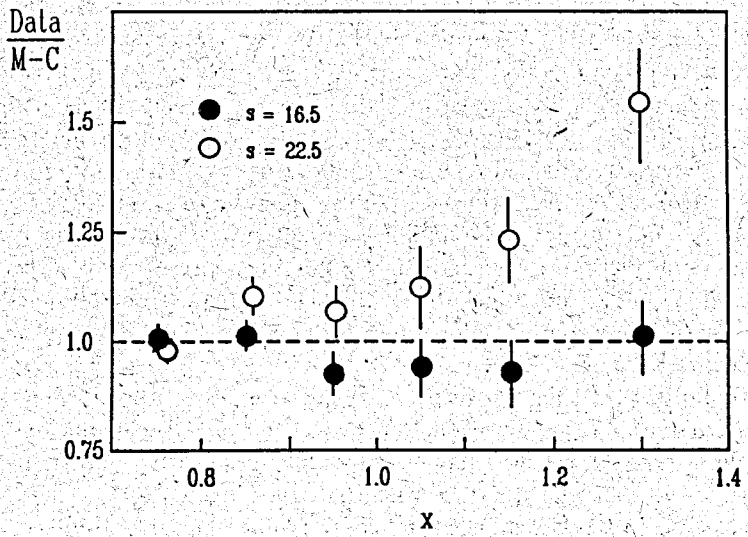

Fig. 6: Ratio of experimental to Monte Carlo event distributions, for two values of the parameter s.

measured ones only at $x > 0.75$:

$$F_2^C(x,Q^2) = F_2^f(x,Q^2), \quad x \leq 0.75 \tag{7}$$

$$F_2^C(x,Q^2) = F_2^f(x=0.75,Q^2)\exp(-s(x-0.75)), \quad x > 0.75 \tag{8}$$

where F_2^f is a polynomial parametrization of the measured F_2^C from ref. [1] and s is a free parameter. The exponential dependence of F_2^C at large x is predicted in certain theoretical models which describe nuclear effects in structure functions by multiquark clusters [19, 20, 21, 22] or few nucleon correlations in nuclei [23].

Varying the parameter s between 6 and 22.5 in eqn. (8), we have compared Monte Carlo and experimental event distributions $dN_r(x')/dx'$, integrated over $Q^{2\prime}$. The variation of the χ^2 of this comparison with s is shown in Fig. 5. The best agreement, taking into account statistical errors only, was observed for $s = 16.5^{+0.2}_{-0.2}$, with a $\chi^2/d.o.f. = 4.0/5$. The corresponding ratio of experimental and simulated events is shown in Fig. 6 and is found to be compatible with unity.

To search for a Q^2 dependence of F_2^C, we have split the data in three Q^2 bins of $52 - 70\,\mathrm{GeV}^2$, $70 - 100\,\mathrm{GeV}^2$, and $100 - 200\,\mathrm{GeV}^2$. The resulting F_2^C at the three bin centers is given in Table 1 and is shown in Fig. 7. In each Q^2 bin, F_2^C has been fitted with an exponential $\exp(-sx)$. The resulting fit parameters are shown in Table 2. Within the errors, we observe no dependence of s on Q^2. The data are, however, also compatible with a small Q^2 dependence of F_2^C (scaling violation) which is predicted by perturbative QCD and which is clearly established at smaller values of x [1].

The systematic uncertainties of our data are discussed in detail in section 6 below. The systematic error on s was obtained by modifying the measured F_2^C for the effect of each individual source of systematic error in turn and repeating the fit. The corresponding individual variations of s were then combined in quadrature. Since the resolution of the spectrometer deteriorates rapidly with increasing x, only upper limits on F_2^C have been obtained for $x \geq 1.15$.

To establish the presence of nuclear effects in F_2^C, we have compared our data to predictions of conventional nuclear Fermi motion calculations. As an example, we have used the model of ref. [24], simulating the distribution of reconstructed events $dN_r(x')/dx'$ with the trial F_2^C of equs. (7, 8), where s is defined as $s = \ln K(Q^2)$ and where K is a polynomial used to approximate the

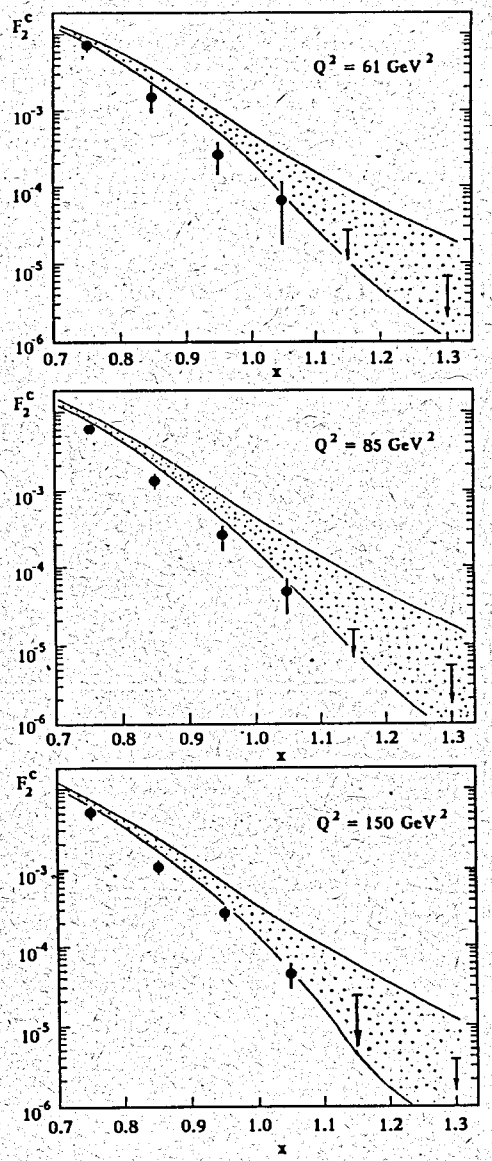

Fig. 7: The nuclear structure function $F_2^C(x)$ as a function of x, at three different values of Q^2. The hatched regions show the range of predictions of ref. [26].

calculations of ref. [24]. The comparison with the experiment is shown in Fig. 8a. The Monte Carlo simulation reproduces the experimental $dN_\tau(x')/dx'$ in the range $0.4 < x < 0.8$, confirming the good agreement between the present analysis and the one of ref. [1]. The data start to disagree with the Monte Carlo simulation at $x = 0.8$. The overall χ^2 of the comparison amounts to 33.0 for 9 degrees of freedom. We conclude that at $x > 0.8$ the data exhibit a nuclear effect which is not described by conventional models of Fermi motion.

6 Systematic errors

The most important effects which lead to systematic errors on $F_2^C(x, Q^2)$ are uncertainties on

- the magnetic field of the spectrometer,
- the incident muon energy E,
- the spectrometer resolution,
- detector inefficiencies,
- the absolute cross section normalization.

Many other sources of systematic errors have also been considered.

The magnetic field of the spectrometer has been calibrated with a global uncertainty of 0.15% [1]. The corresponding uncertainty on $F_2^C(x, Q^2)$ is presented in Table 1 as a multiplicative factor f_s.

The uncertainty in the incident muon energy E at the interaction vertex originates from two sources: (a) from the spectrometer measuring the momentum of the incident muons upstream of the apparatus and (b) from the corrections for the energy loss ΔE in the carbon target. The first uncertainty amounts to 0.15%. The accuracy of the calculations of ΔE is of the order of 1% and the largest energy loss in the target was about 7%, such that the uncertainty in E due to the ΔE correction is between 0 and 0.07% depending on the vertex coordinate. These uncertainties can change $F_2^C(x, Q^2)$ at x=1.0 by 15% at $Q^2 = 61\,\mathrm{GeV}^2$ and by 3.5% at $Q^2 = 150\,\mathrm{GeV}^2$. They are shown in Table 1 as a factor f_b.

To estimate uncertainties from the spectrometer resolution, we have considered separetely the central region of the resolution function of the spectrometer, and its tails. The width of the central region has been checked with calibration runs where beams of known energy were sent directly into the spectrometer. From a Monte Carlo simulation of such calibration runs, we estimate that the systematic uncertainty on the width of the central part of the resolution function in x is less than 5%. This error was introduced in turn into the Monte Carlo simulation of the experimental data to obtain an $F_2^{C\prime}$ different from F_2^C by a factor f_r which is also given in Table 1.

The calibration runs did not yield sufficiently accurate information about the tails of the spectrometer resolution function which are mainly caused by Coulomb scattering at large angles. Uncertainties due to a possible underestimate of such tails have been evaluated with the help of a Monte Carlo program where multiple Coulomb scattering is simulated following the Moliere theory, i.e. it includes a detailed treatment of large angle scattering and thus accounts for long range correlation effects. This was compared to our results based on the Monte Carlo simulation with the standard GEANT algorithm where multiple scattering is treated in the Gaussian approximation. As expected, these different treatments do indeed lead to different predictions for the spectrometer resolution in various kinematic variables (Fig. 9). However, since these differences appear only in the far distant tails of the resolution functions, they give rise to differences in the reconstructed event distributions which are insignificant when compared to the statistical errors. The ratio of the two corresponding event distributions is shown in Fig. 10, from which we conclude that systematic errors on F_2^C due to an underestimate of large angle scattering in the spectrometer resolution does not exceed 15% for $x < 1.2$.

Uncertainties in the MWPC and trigger counter efficiencies were estimated to be 0.5% and 0.3%, respectively. The resulting uncertainties in $F_2^C(x, Q^2)$ are below 0.3% at $x = 1.0$. They are shown in Table 1 as a factor f_d and are very small when compared to the other errors. The absolute normalization uncertainty of the data is estimated to be smaller than 3% [1].

To search for possible other experimental uncertainties, the structure function $F_2^C(x, Q^2)$ has been evaluated in bins of the vertex position and of the azimuth angle. Also the effect of kinematical cuts has been carefully studied. In all cases, no variations beyond the statistical fluctuations have been observed.

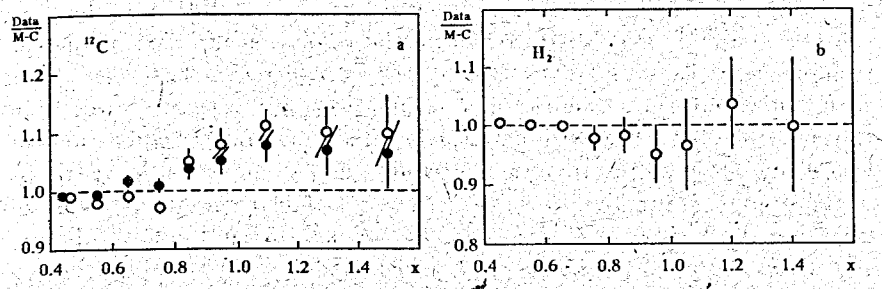

Fig. 8: Comparison of the experimental and Monte Carlo event distributions for the experiments with a carbon (a) and a hydrogen target (b). Two parametrisations of nucleon structure functions have been used in the Monte Carlo simulation of the carbon target data: F_2^N without nuclear effects (open points) and F_2^C corrected for Fermi motion with the prescription of ref. [24] (closed points).

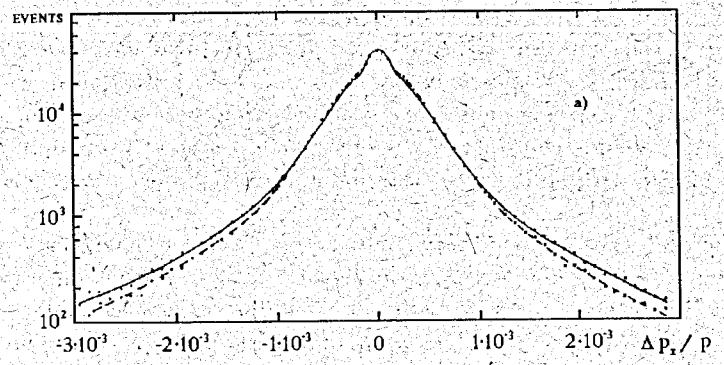

Fig. 9: Momentum resolutions $\Delta p_x/p$ (a) and $\Delta p_z/p$ (b) for two components of the momentum vector of the scattered muon; p_z is the momentum component along the direction of the incoming beam. The resolutions are shown for two different Monte Carlo simulations treating multiple Coulomb scattering in the Moliere theory (full line) and in a Gaussian approximation (dashed line).

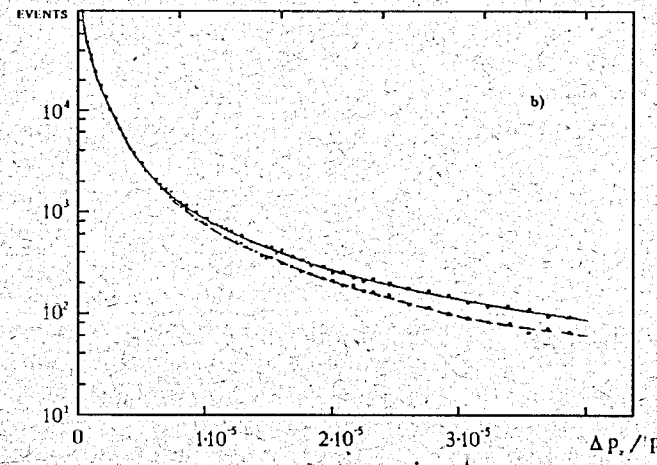

Fig.9b

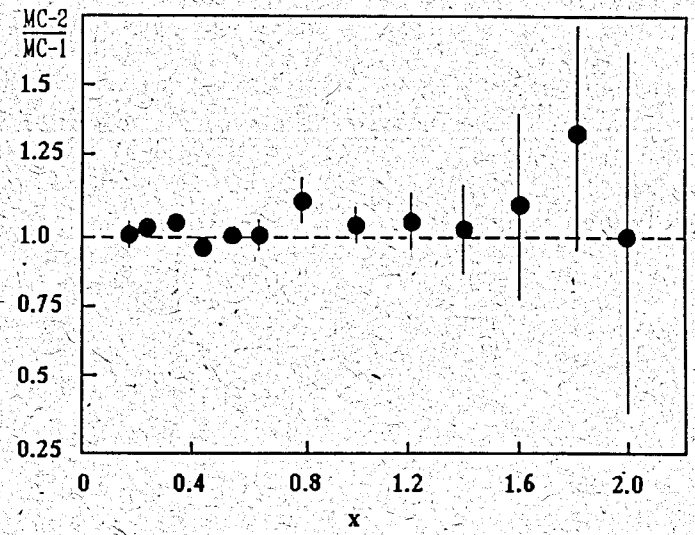

Fig.10: Comparison of the reconstructed events distributions generated using the Moliere (MC-2) and Gaussian (MC-1) treatment of multiple Coulomb scattering.

In order to convince ourselves that the nuclear effects observed in the large x region are not faked by resolution or other systematic effects, we have repeated the same analysis on our data taken with a liquid hydrogen target under otherwise identical experimental conditions, and with the same beam energy of 200 GeV [2]. In contrast to the carbon data, the free proton data are well described by the Monte Carlo simulation ($\chi^2/d.o.f. = 5.4/9$) (Fig. 8b). This demonstrates the good understanding of the spectrometer resolution. If the discrepancy between the carbon data and the Monte Carlo simulation at large x (Fig. 8a) were due to an underestimate of resolution smearing or other experimental effects, the same discrepancy would have been observed in our hydrogen data which differ from the carbon data only in the target material. As in the case of the carbon data, the proton structure functions $F_2^p(x,Q^2)$ from the present analysis and from the analysis described in [2] agree well in the overlap region $0.4 < x < 0.8$.

7 Discussion of results

The structure function $F_2^C(x,Q^2)$ at $x = 1$ obtained in the present experiment amounts to $(1.2^{+0.4}_{-0.6}) \cdot 10^{-4}$ in our Q^2 range (Fig. 7). This value can be compared to a wide spectrum of theoretical models [25, 26, 27, 28, 29] for $F_2^C(x=1)$ which give predictions in the range $10^{-5} < F_2^C < 10^{-3}$. The predictions of ref. [28] and [29] are excluded by our data. The data agree well with the quark cluster model of ref. [25] where $F_2^C(x,Q^2)$ is treated as the sum of pure nucleon and six-quark components, the admixture of the six-quark clusters amounting to about 5%.

In Fig. 7, we compare our data to the calculations of Frankfurt and Strikman [26] who predict the existence of few nucleon correlations inside a nucleus. Depending on the strength of such correlations, their model gives a range of predictions for $F_2^C(x)$ which are shown by the shaded areas in Fig. 7. We conclude that the data are in reasonable agreement with this model.

In the model of ref. [27] the nuclear structure function $F_2^A(x)$ is described as the sum of the free nucleon structure function and of an exotic component which is due to the quark dynamics in the short distance interactions between two nucleons in a nucleus. Fermi motion of both the nucleons and of the exotic component is taken into account. The prediction of the model for $F_2^C(x)$ obtained at $Q^2 = 60 GeV^2$ is very close to the lower boundary of the shaded region in Fig. 7 and thus also agrees with the data.

8 Conclusion

We have presented the first measurement of the nuclear structure function $F_2^C(x,Q^2)$ at high Q^2 ($Q^2 > 52\,\mathrm{GeV}^2$) and x ($0.8 < x < 1.3$) from deep inelastic muon-carbon scattering. The observed $F_2^C(x,Q^2)$ in the region of $x = 1.0$ is too large to be explained in the framework of conventional Fermi motion models. The structure functions obtained can be fit by an exponential $F_2^C(x) \propto \exp(-sx)$ with $s \approx 16$. No Q^2 dependence of s is observed within the accuracy of this experiment. The results on $F_2^C(x,Q^2)$ are consistent with models which predict nuclear effects near the single nucleon kinematic limit from few nucleon correlations, multiquark clusters, or exotics.

9 Acknowledgements

We would like to thank J. Strachota, G. Todorova and P. Todorov for invaluable help with the data taking and data analysis, R. Brun, and M. Goossens for their contribution to the software development, and A.A. Akhundov, D.Yu. Bardin and N.M. Shumeiko for their contributions to the radiative corrections procedure.

References

[1] BCDMS, A.C. Benvenuti et al., Phys. Lett. B195 (1987) 91.

[2] BCDMS, A.C. Beuvenuti et al., Phys. Lett. B223 (1989) 485.

[3] BCDMS, A.C. Benvenuti et al., Phys. Lett. B237 (1990) 592.

[4] EMC, J.J. Aubert et al., Nucl. Phys. B259 (1985) 189.

[5] EMC, J.J. Aubert et al., Nucl. Phys. B272 (1986) 158.

[6] EMC, J.J. Aubert et al., Nucl. Phys. B293 (1987) 740.

[7] L.W. Whitlow et al., Phys. Lett. B250 (1990) 193;
L.W. Whitlow et al., Phys. Lett. B282 (1992) 475.

[8] NMC, P. Amaudruz et al., Phys. Lett. B295 (1992) 159.

[9] CCFR, S.R.Mishra et al., Nevis Report No 1459.

[10] CDHSW, P. Berge et al., Z. Phys. C49 (1991) 187.

[11] BCDMS, G. Bari et al., Phys. Lett. 163B (1985) 282;
BCDMS, A.C. Benvenuti et al., Phys. Lett. 189B (1987) 483;
R.G. Arnold et al., Phys. Rev. Lett. 52 (1984) 727.

[12] B.W. Filippone et al., Phys. Rev. C 45 (1992) 1582;
P. E. Bosted, Phys. Rev. C 46 (1992) 2505.

[13] G. Altarelli and G. Martinelli, Phys. Lett. B76 (1978) 89.

[14] BCDMS, D. Bollini et al., Nucl. Instr. Meth. 204 (1983) 333.

[15] R.Brun, CERN-DD/EE/79-3 (1979).

[16] R. Brun et al., CERN-DD/EE/78-1 (1978);
R. Brun et al., CERN-DD/78-2 (1978).

[17] W. Lohmann, R. Kopp and R. Voss, CERN 85-03, 1985 (CERN Yellow Report).

[18] A.A. Akhundov et al., Sov. J. Nucl. Phys. 26 (1977) 660; *ibid.* 44 (1986) 988;
A.A. Akhundov et al., Sov. J. Nucl. Phys. 44 (1986) 988;
D.Yu. Bardin and N.M. Shumeiko, Sov. J. Nucl. Phys. 29 (1979) 499;
A.A. Akhundov et al., JINR Communications E2-86-104, Dubna 1986.

[19] A.M. Baldin et al., Proc. Rochester Meeting APS/DPF, New York 1971, pp. 131–137;
A.M. Baldin et al., Sov. J. Nucl. Phys. 18 (1974) 41.

[20] A. Krzywicki, Nucl. Phys. A446 (1985) 135.

[21] L.A. Kondratyuk and M. Zh. Shmatikov, Yad. Fiz. 41 (1985) 222; Letters to ZhETF 39 (1984) 324.

[22] T. Fujita, J. Hufner, Nucl. Phys. A343 (1980) 493.

[23] L. Frankfurt and M. Strikman, Phys. Rep. 76 (1981) 216.

[24] A. Bodek and J.L. Ritchie, Phys. Rev. D24 (1981) 1400.

[25] L. Kaptari and A. Umnikov, JINR Rapid Communications 32 (1988) 17.

[26] L. Frankfurt and M. Strikman, Phys. Rep. 160 (1988) 325.

[27] S. Date et al., Phys. Rev. Lett. 52 (1984) 2344;
K. Saito and T. Uchiyama, Z. Phys. A322 (1985) 299.

[28] A.I. Titov, Yad. Phys. 38 (1983) 1582.

[29] A. Efremov and E. Bondarchenko, JINR Communications E2-84-124, Dubna 1984.

Received by Publishing Department
on April 14, 1993